

Panoptic Image Annotation with a Collaborative Assistant

Jasper R. R. Uijlings
Google Research
jrru@google.com

Mykhaylo Andriluka
Google Research
mykhayloa@google.com

Vittorio Ferrari
Google Research
vittoferri@google.com

Abstract

This paper aims to reduce the time to annotate images for panoptic segmentation, which requires annotating segmentation masks and class labels for all object instances and stuff regions. We formulate our approach as a collaborative process between an annotator and an automated assistant who take turns to jointly annotate an image using a pre-defined pool of segments. Actions performed by the annotator serve as a strong contextual signal. The assistant intelligently reacts to this signal by annotating other parts of the image on its own, which reduces the amount of work required by the annotator. We perform thorough experiments on the COCO panoptic dataset, both in simulation and with human annotators. These demonstrate that our approach is $5\times$ faster than manual polygon drawing tools, and is also significantly faster than the recent machine-assisted interface of [5]. Furthermore, we show on ADE20k [59] that our method can be used to efficiently annotate new datasets, bootstrapping from a very small amount of annotated data.

1. Introduction

This paper aims to reduce the time it takes to annotate images for the panoptic segmentation task. This requires annotating segmentation masks and class labels for all object instances and stuff regions. Such annotations are expensive: it took 19 minutes for a single image for COCO [14, 38] and 1.5 hours for Cityscapes [20]. In this paper we propose to reduce annotation time by learning to predict how the image should be annotated.

To this end we formulate our approach as a collaborative process between a human annotator and an automated assistant agent who take turns to jointly annotate an image. To see this process in action, Fig. 1a shows an example image and Fig. 1b the current annotation, which is partially machine generated. At this point, the annotator converts one of the *road* segments into *pavement*. The assistant reacts by changing the labels of similar looking segments elsewhere in the image to *pavement* as well. Fig. 1e and 1f show another example image and current annotation. After the an-

notator corrects the *cup* to be a *bowl*, the assistant automatically adds another *bowl*, as well as a *spoon*, a *bottle*, and a *wooden floor*. This significantly helps the annotator.

We build on [5], which proposed to annotate an image by composing segments out of a pre-defined pool, using an interface in which annotators can repeatedly perform one of the following actions: add a segment from the pool, change the label of a segment, and remove a segment. In this paper we introduce an automatic assistant which helps the annotator by executing some of these actions on its own. Crucially, whenever the annotator performs an action, this directly provides a ground-truth annotation for a segment. This ground-truth serves as a strong form of context, stronger than the use of *predicted context* in previous works [27, 29, 37, 42, 44, 49, 55]. We propose an assistant that reacts intelligently to annotator actions by capitalizing on these strong contextual cues to automatically improve the annotation of other parts of the image.

To summarize, we introduce a framework in which an assistant and an annotator collaboratively annotate an image. The assistant intelligently reacts to annotator input based on context by annotating other parts of the image on its own. We experimentally demonstrate that: (1) in simulations on the COCO panoptic dataset [14, 32, 38] our method is 17% – 27% faster than [5]; (2) studies with human annotators on this dataset confirm this and enable to compare to manual polygon drawing, revealing that our method is $5\times$ faster. (3) a cross-dataset experiment on ADE20k [59] shows that our method can be used to quickly annotate new datasets, bootstrapping from a very small amount of labeled data.

2. Related Work

Interactive Segmentation. Many works address interactive object segmentation. Most classical approaches [6, 8, 11, 50, 21, 18, 24, 45] cast the problem as an energy minimization function defined on a graph which spans over pixels. Many recent methods adapt Fully Convolutional neural networks (FCNs, e.g. [16, 39]) for single object segmentation by using user scribbles or clicks as additional input signal [9, 29, 34, 35, 36, 40, 41, 58]. In [17] they use an FCN

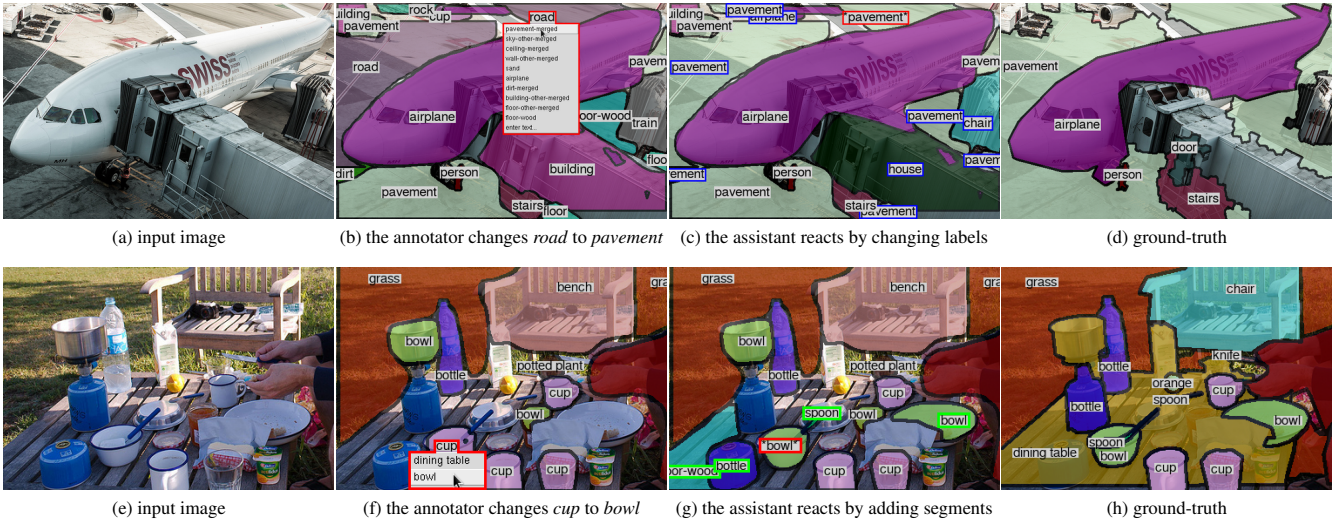


Figure 1. Example of the collaborative annotation process. Given an input image, the human annotator and the automated assistant carry out actions in turn. Based on the current annotation, the annotator performs one action (highlighted in red). Then the assistant reacts with by changing labels (in blue) and adding segments (in green). For comparison we show the ground-truth panoptic segmentation.

to produce pixel-wise embedding space. They combine this with scribbles or clicks and a nearest neighbour classifier to segment objects within video. Polygon-RNN [3, 15] is a recurrent neural net which predicts polygon vertices which an annotator can adjust. In [34] they predict object boundaries using an FCN which accepts boundary clicks, which they turn into an instance using a geodesic path solver [19].

While the vast majority of works focuses on individual objects, a few recent works have started to tackle the full image annotation problem [5, 4]. In [4] they do class-agnostic segmentation of all objects in an image starting from extreme points [46] followed by corrective scribbles. The closest related work to ours is Fluid Annotation [5]. Instead of segmenting one object at a time, they propose an interface to quickly annotate a complete image by composing segments out of a pre-defined pool. The interface is designed to make it easy for the annotator to perform the action she chooses. In this work we build on top of [5] and go beyond by introducing an automated assistant that performs some annotation actions on its own.

Assign annotation tasks. A few works propose to intelligently choose what annotation task to send to the annotator [33, 56, 52]. In [33] they focus on creating a bounding box for each image-label pair. They have an agent decide whether to ask the annotator to draw a bounding box [46, 54] or verify whether a machine-generated bounding box is good enough [47]. In [52] the machine dispatches annotation tasks to optimize the trade-off between the annotation budget and the final labeling quality. Tasks include providing image labels, providing a label for a certain box, verify a box, draw boxes around other instances of the same class, etc. In [56] they estimate the informativeness and cost of having an image label, a box, or a full segmentation

of an image, which they use to dispatch these tasks in an active learning framework. In these works the machine decides which tasks to send to the annotators while the tasks themselves are not interactive. In our case there is a single interface through which both the machine and the annotator interactively take turns.

Other works on interactive annotation. In [51] they created a semantic segmentation network which can consume natural language input. This enables a user to correct a machine-predicted segmentation by giving instructions in English. In [12] they propose a framework to convert bounding boxes, instance masks, and part annotations into each other using human verification and human corrections. Other works address fine-grained classification, where annotators provide feedback or correct the classifiers based on attributes [13, 48, 10, 57].

3. Overview

Given an input image we want to produce a dense labelling of every pixel with a semantic label and object identity. This includes “thing” classes corresponding to various countable objects, and “stuff” classes corresponding to uncountable classes which typically occupy background areas. Example annotations are shown in Fig 1d and 1h.

We start from the recent Fluid Annotation interface [5] that allows to quickly annotate an image by composing segments out of a pre-defined pool (Sec. 3.1). In this paper we turn this into a collaborative environment (Sec. 3.2) and introduce an automated assistant which helps the annotator complete its task (Sec. 3.2). Crucially, every action of the annotator provides strong contextual cues which the assistant uses to predict how the image should be annotated. Then the assistant *carries out some actions on its own*.

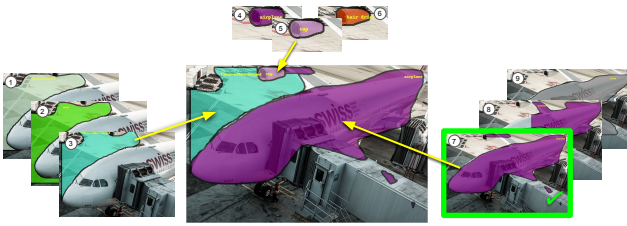


Figure 2. The *proposal set*, *active set* and *fixed set*. The *proposal set* is the complete segment pool created by Mask-RCNN (only a few shown for clarity). The *active set* defines the current annotation (segments 3, 5, 7 here). The *fixed set* contains segments which were modified or added by the annotator and are considered to be ground-truth (only segment 7 here).

3.1. Fluid Annotation [5]

Fluid Annotation [5] starts by generating a *proposal set* of segments with accompanying class labels using Mask-RCNN [25]. They modified Mask R-CNN to generate about 1000 segments per image, which is more than usual, and to produce segments also on stuff classes (not only on things). The annotator can annotate the image by selecting an ordered subset of these proposals and by optionally correcting their labels. The proposals are ordered to ensure that a single pixel is assigned to only one segment, following the definition of panoptic segmentation [32].

From the proposal set, the work of [5] first creates an initial annotation for the whole image using an iterative greedy algorithm [5, 32]. Starting from the empty image, first the highest scored segment is selected. Then the next-highest scored segment is placed behind all other segments, if enough of its surface is visible. This algorithm creates an initial ordered *active set*. This active set is a subset of the proposal set, and defines the current annotation (Fig. 2). The annotator can modify the active set by performing four kinds of actions: *add a segment* from the proposal set into the active set, *remove a segment*, *change label* of an active segment, and *change depth order* of an active segment.

The Fluid Annotation interface facilitates the actions made by the annotator: when adding a segment, the interface uses the mouse position to make a small, ordered selection of segments for the annotator to quickly scroll through. When changing a label, the interfaces makes a shortlist of likely labels for that segment. Hence in [5] the system facilitates the annotator to perform the one action she chose.

3.2. Collaborative fluid annotation

In this paper we want to extend the influence of each annotator action beyond the one segment that was targeted. We achieve this by introducing an *automatic assistant* to the Fluid Annotation system. We model annotation as a collaborative environment in which the annotator and the assistant alternate in taking turns, where both use the same set of actions. Conceptually, the annotator has perfect knowledge about the visual world and about the annotation it aims to

achieve. However, it has only partial view of the proposal set, and exploring this set is a costly process. Conversely, the assistant can access all the proposal segments instantly, but has limited capability to judge which proposals belong to the final segmentation the human annotator would like to achieve. The aim of the annotator is to produce a high-quality panoptic annotation. The goal of the assistant is to reduce the overall annotation effort.

Crucially, the annotator conveys his knowledge about the world through every action she takes, essentially creating ground-truth as she goes. This freshly created knowledge provides strong contextual cues which the assistant uses to predict how the rest of the image should be annotated. This enables the assistant to react to the annotator and carry out some actions on its own.

Fixed Set. To establish communication between the annotator and the assistant we introduce a *fixed set*. It contains all segments which have been approved by the annotator and are considered to be ground-truth. It is a subset of the active set, which in turn is a subset of the proposal set (Fig. 2).

The fixed set is created without any additional costs. Whenever the annotator changes the label of a segment, the segment is correct semantically (by construction) and geometrically (otherwise it would have been better to remove the segment). Whenever the annotator adds a segment, it is geometrically correct. Furthermore, if its label is incorrect, the natural behaviour of the annotator is to correct it immediately afterwards. So we can safely put a newly added segment into the fixed set if the next action of the annotator does not correct its label. Hence segments added by the annotator end up in the fixed set with a delay of one action.

Since the fixed set can be considered as ground-truth, we do not allow the assistant to make any changes to it.

The assistant and the annotator take turns to collaboratively annotate an image. In our framework, the assistant performs as many actions as it wants to, until it decides stop. Then the annotator performs one action. If this action alters the fixed set, the assistant has more information which it can use during its next turn.

We introduce a collaborative assistant in Sec. 3.3. This assistant reacts to context provided by the annotator and can perform the *change label* and *add* actions. We also introduce an initialization agent in Sec. 3.4. It acts before the annotator and replaces the greedy initialization stage of Fluid Annotation (Sec. 3.1).

3.3. Collaborative Assistant (CA)

Our collaborative assistant automatically performs actions to accelerate the annotation process. To identify useful actions, it relies on a *context model* that captures dependencies between fixed segments and the segments in the proposal set. Here we describe the action generation process of the assistant, and then present details of the context model.

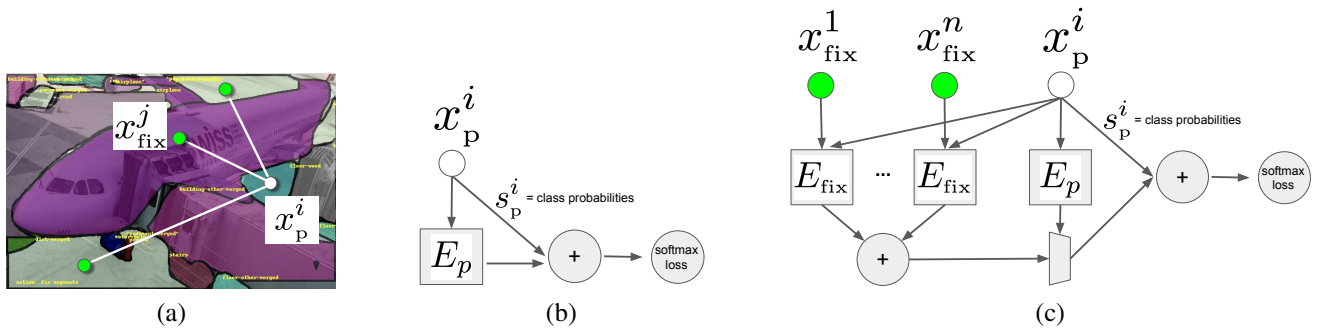


Figure 3. (a) Example image with three fixed segments (green dots), and a proposal segment (white dot). (b) Diagram of a simple model with skip connections that does not have access to fixed segments. (c) Diagram of our context model.

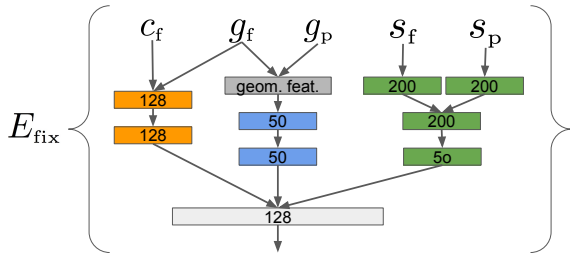


Figure 4. Structure of the E_{fix} subnetwork. Each of the rectangular blocks corresponds to a fully connected layer with ReLU activation. The number inside each block indicates the number of outputs. The module first independently processes geometric, appearance and human-provided inputs using the layers shown in blue, green and orange respectively and then fuses all inputs together in the final layer (light gray). For simplicity the variable names do not include indices of fixed and proposal segments.

Action generation. Denote the fixed set as X_{fix} . For the *change label* action, our context model predicts $p(c_p^k | X_{fix})$ for each segment k . The collaborative assistant generates a *change label* action when the highest scored label of the context model is different from the current label. The action updates the label to m , using $\arg \max_m p(c_p^k = m | X_{fix})$.

Similarly, for the *add* action our model predicts $p(d_p^k | X_{fix})$. The *add* action is generated whenever $p(d_p^k | X_{fix})$ is greater than a threshold τ , and the segment k is not yet in the active set. In practice we set $\tau = 0.9$ as estimated on a validation set (Sec. 4).

Context model. For both actions we use a context model with the same architecture. Let the set of fixed segments be denoted by $X_{fix} = \{x_{fix}^k | k = 1, \dots, K\}$ and the set of proposal segments by $X_p = \{x_p^i | i = 1, \dots, N\}$.

In our model the features of the fixed and proposal segments are given by $x_{fix}^k = [c_f^k, g_f^k, s_f^k]$ and $x_p^i = [g_p^i, s_p^i]$ respectively. Each of the variables g_f^k and g_p^i corresponds to a 4D vector encoding the center of the segment and the width and height of its bounding box. This captures spatial relationships between the proposals. The variables s_f^k and s_p^i each correspond to a vector of class scores (i.e. logits) assigned to the segment by Mask-RCNN. These logits cap-

ture semantic information and, since they are linear projection of the final feature vectors, they also contain information about the segments’ appearance. Finally, the variable c_f^k denotes a one-hot encoding of the segment class that has been assigned to the fixed segment by the human annotator. Note that the c_f^k component of the fixed segment representation x_{fix}^k provides an additional and potentially strong cue for resolving ambiguities in the label of the proposal segments. This is a new piece of information not accessible to Mask-RCNN as usually deployed (i.e. without a collaboration with a human).

The structure of our *change label* context model is shown in Fig. 3 (c). Our starting point is a simple update model shown in Fig. 3 (b). This model takes the segment features x_p^i as input and computes incremental updates to the class probabilities using a fully connected neural network E_p , similarly to a single layer in the ResNet model [26]. We extend this simple model with a graph-convolutional [31] sub-network that computes a fixed-size vector summarizing the relationship between the proposal and the unordered, arbitrarily sized, fixed set:

$$\bar{E}_{fix} = \frac{1}{K} \sum_k E_{fix}(x_p^i, x_{fix}^k). \quad (1)$$

The output of \bar{E}_{fix} is then combined with the output of E_p and is passed through a single fully connected layer to compute a difference vector with respect to the original class probabilities of a proposal segment x_p^i .

Our context model for the *add* action is almost identical in structure. But instead of updating all class scores s_p^i it only updates the highest class score while the softmax loss is replaced by a binary cross-entropy loss (present/absent).

In Fig. 4 we show the structure of the component E_{fix} that encodes relationship between a fixed segment and a proposal segment. We follow the late fusion strategy and first apply a series of transformations to each type of input features before finally combining them together. Prior to feeding geometric features g_f and g_p into the network, we transform them into a 10-dimensional vector of relative features defined similarly to [28]. Let us denote the offset vector between the locations of the fixed and

the proposal segment as Δ_{fp} , and after normalization by the width and height of the fixed segment as $\hat{\Delta}_{fp}$. The vector of relative geometric features is then obtained by concatenating Δ_{fp} , $\log(|\hat{\Delta}_{fp}|)$, $\log(w_p/w_f)$, $\log(h_p/h_f)$, $\text{sign}(\Delta_{fp}) \log(|\Delta_{fp}|)$, and $\text{sign}(\Delta_{fp}) \log(|\hat{\Delta}_{fp}|)$.

Local score pooling. The model described above can operate with any type of segment scores s_p^i . We found that instead of directly using the scores provided by Mask-RCNN we achieve higher accuracy by performing a form of max-pooling over the scores of nearby segments. This corresponds to defining a new score vector \hat{s}_p^i as

$$\hat{s}_{p,c}^i = \max_{j \in N(i,c)} s_{p,c}^j \quad (2)$$

where c is a class label, and $N(i, c)$ is the set of segments with label c that have intersection-over-union < 0.5 with segment i .

Training the context model. The ideal training data for our context model would be composed of training examples derived from the actions performed by real humans during image annotation. Since collection of such training data is impractical we use data collected in simulation. To that end we simulate the fluid annotation process for each of the images in the training set using the simulator described in [5] and store all segments and their labels contained in the final annotation. To construct training examples of the fixed set for our context model we then randomly sample correct segments out of the final annotation. We found such random sampling to be necessary to make the model robust with respect to the size of the fixed set encountered by the agent when deployed at annotation time. We train the context model using the Adam optimizer [30].

Discussion. A number of previous works attempt to exploit context based purely on image signals [27, 29, 37, 44, 49, 55]. Instead, our contextual cues are based on *human input*, which makes them much stronger. In terms of technical realization, our context model is related to models used for visual question answering [53] and for modeling relationships between scene objects [28].

3.4. Initialization Assistant (IA)

In the original Fluid Annotation, the initialization was done greedily through non-maximum suppression of Mask-RCNN segments based on their scores [5]. In this section we use an initialization assistant to do this instead. The initialization produces a panoptic segmentation by composing segments from the proposal set, without any human annotator involved. This method therefore can also be used for classical image segmentation prediction [16, 32, 39, 43].

We represent each segment as a feature vector consisting of: (a) an 8-bit encoding of the class label predicted by Mask-RCNN; (b) the predicted score of the segment; (c)

the percentage of the segment surface that does not overlap with any segments in the current active set.

The assistant uses these features to iteratively perform actions, starting from an empty active set. At each time step, it scores all the segments which could be added and select the one with the highest score. If this score is above a certain threshold, it adds the segment to the active set. Otherwise, it stops.

To train our initialization assistant, we collect examples by simulating the full fluid annotation process for each image (as in Sec. 3.3). This results in a set of positive *add* actions with their features. We obtain negative *add* actions with a form of hard negative mining. In particular, at several points during the fluid annotation simulation we ask the initialization assistant to make predictions. All predicted *add* actions which are inconsistent with the original ground truth form the negative example set. As model we use a simple 4-layer fully connected neural net. We use a quadratic hinge loss and train using the Adam optimizer [30].

Our initialization assistant is conceptually related to the search-based structured prediction algorithm [22], and to other approaches that iteratively generate structured outputs one component at a time [23, 7].

4. Results

In this section we first evaluate the context model (Sec. 4.1) and the full collaborative annotation process in simulation (Sec. 4.2). Then we report a study with human annotators (Sec. 4.3) and finish with a cross-dataset experiment (Sec. 4.4).

Dataset. In most experiments we use the COCO panoptic dataset [1], which is a combination of the original COCO dataset [38] and COCO-stuff [14], with some stuff classes merged based on [32]. It contains 118K training and 5K validation images densely labeled with 80 thing and 53 stuff classes. We divide the training set into two equal sized splits, one to train Mask-RCNN and another for our assistants (including the context models). We use the validation set for evaluation.

In Sec. 4.4 we perform experiments on ADE20k to demonstrate that our method can be used to annotate a new dataset (see detailed protocol in that subsection).

4.1. Context model

In this section we evaluate the performance of our context model in isolation. We measure how well it can correct labels predicted by Mask-RCNN, given a set of fixed segments X_{fix} .

Protocol. Given an image and the ground-truth segmentation, we first select the set of Mask-RCNN proposals E which best match the ground-truth segments geometrically. We do this by greedily selecting proposal segments that have maximal IoU with a ground-truth segment. We then

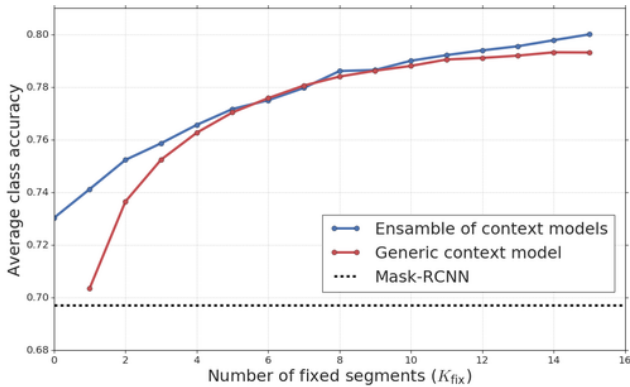


Figure 5. Class label accuracy delivered by our context model (red, blue) as a function of the number of fixed segments given to it. The Mask-RCNN baseline (dashed black) represents the starting point without context model. Note that for $K_{\text{fix}} = 0$ the accuracy of the ensemble model is higher than the baseline due to local score pooling (Eq. (2)).

measure the initial label accuracy provided by Mask-RCNN on these selected proposals E , and compare it to the accuracy after re-labeling them with the context model. We do this on 4500 COCO validation images (out of 5000) and measure accuracy averaged over classes.

When applying our context model, for each segment $s \in E$ we randomly select a fixed set of other segments in $X_{\text{fix}} \in E \setminus s$. We evaluate over a range of different number of fixed segments $|X_{\text{fix}}|$ and each time measure accuracy over all other segments. For this experiment we train a single *generic context model* which works for any size of the fixed set. Since this may be sub-optimal, we also train a separate context model for each specific fixed set size, and then combine them into an *ensemble model*.

Results. As Fig. 5 shows, our context model helps improve label prediction accuracy, and its effect grows with the number of fixed segments given to it. For example, when given 8 fixed segments the accuracy increases from 69% for the original Mask-RCNN to 78% with our context model. This demonstrates that the fixed segments provide a strong context signal. We note that this effect is greater than what typically demonstrated in classical context works, which do not benefit from conditioning on human input for parts of image [27, 29, 37, 42, 44, 49, 55].

We also observe that our ensemble model always performs better or equal to our generic model, where the difference is especially large for $K_{\text{fix}} \leq 3$. The ensemble model takes into account the size of K_{fix} and exploits the fact that, intuitively, the more fixed segments are given, the stronger the context signal and thus the more it can be relied upon to alter the labels of other segments.

4.2. Collaborative annotation process

We now evaluate our assistant in the full collaborative annotation environment. We simulate an annotator that tries to reproduce the original ground-truth of the COCO panop-

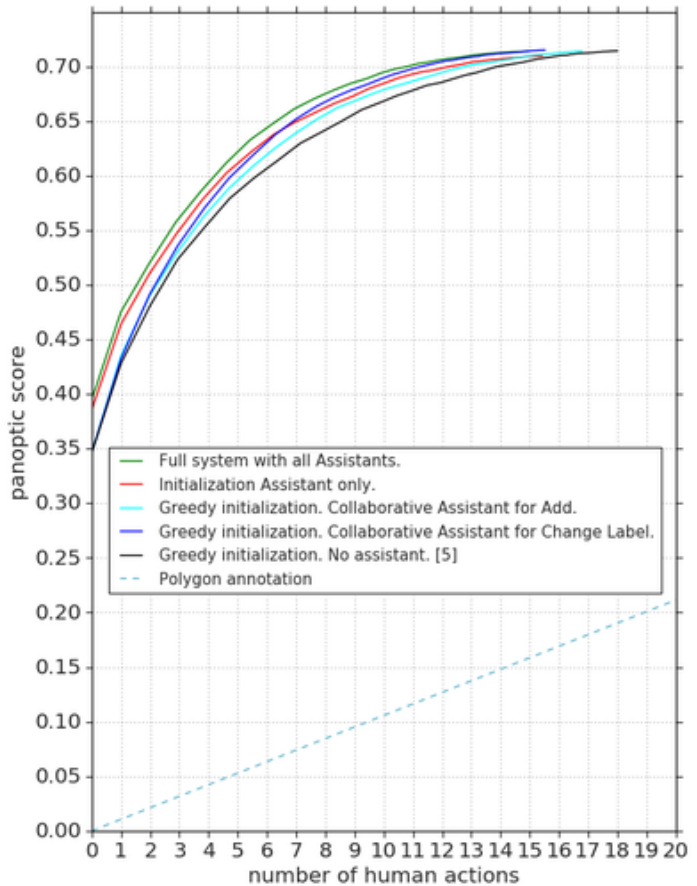


Figure 6. Trade-off between effort and quality for our annotation system. The black line shows the baseline system [5]. The green line is our full system. The other lines are an ablation which evaluates each type of assistance in isolation.

tic challenge [14, 38]. To keep the experiment fully rigorous, we do not report results on the 4500 validation images used to evaluate the context model, but on the remaining 500 images instead.

Results are presented in Fig. 6, which measures quality (panoptic score [32]) as a function of annotation effort (number of human actions). We compare to polygon annotation, where the relation between annotation time and our number of actions is derived from our human user study in Sec. 4.3. We also compare to the original Fluid Annotation system [5] (i.e. greedy initialization and no assistants).

Starting from the greedy initialization, we now introduce two collaborative assistants: one which performs only the *add segment* action, and another which performs only the *change label* action. Since they act after the annotator has performed at least one action, they start from the same point as the greedy initialization. Afterwards, both consistently improve upon the baseline over the full range of the curve. Note how the *change label* assistant has a stronger effect. Intuitively, this makes sense since changing the label of an existing segment is easier than adding a new segment.

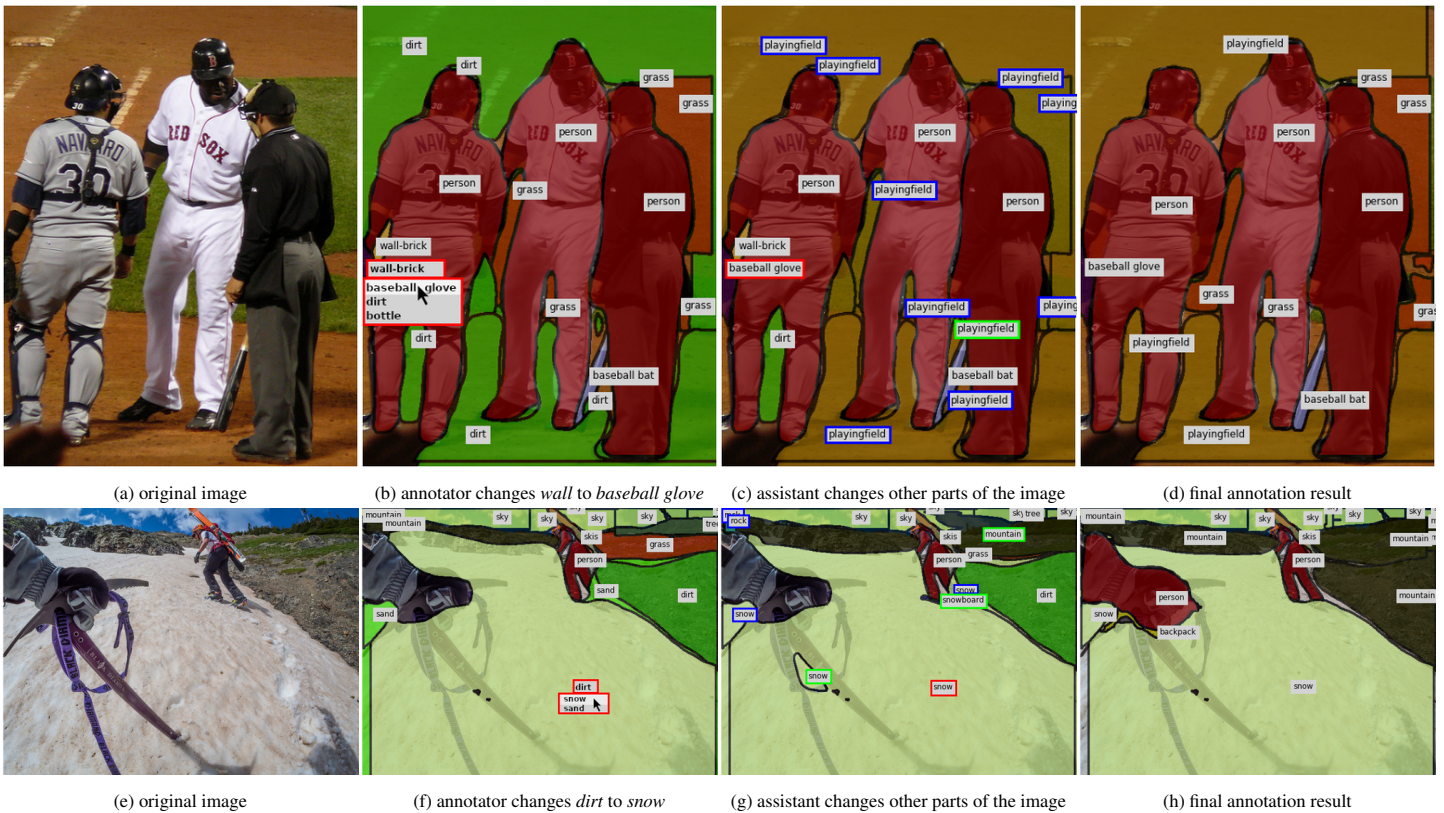


Figure 7. Two examples of the annotation process. When the annotator changes a label (highlighted in red), the assistant reacts by changing labels of existing segments (in blue) and adding new segments (in green).

Another way to improve performance is to use our initialization assistant instead of greedy initialization (Sec. 3.4), which yields a 4% absolute increase in panoptic score (red curve). This suggests that our initialization assistant is a good way to assemble a panoptic segmentation out of Mask-RCNN segments, without any humans involved. It results in a curve which is consistently above the baseline, even without using any further assistance after initialization. At around 7 human actions, it is overtaken by the blue curve of the collaborative change label assistant (starting from greedy initialization).

Finally, we combine all assistants in our full system: the initialization assistant and the collaboration assistant performing both *add* and *change label* (green curve). The full system performs even better than all other variants. It only needs 6.2 annotator actions to deliver 0.65 panoptic quality, whereas the baseline [5] requires 8.5 actions, a speed-up of 27%. Similarly, to obtain the maximum panoptic quality of 0.71, our full system requires 14.9 annotator actions vs 18.0 required by [5], a speed-up of 17%.

When comparing to manual polygon drawing, at 14.9 actions it only results in 0.16 panoptic quality, substantially lower than our method. While using polygons will eventually lead to very complete and high-quality annotations, this will take a very long annotation time.

To better understand how the assistants react to human input, Fig. 7 shows two examples of the collaborative an-

notation process in our full system. Notice the contextual response of the assistant: In the top row, once the annotator has annotated the small *baseball glove*, our assistant changes many regions in the background to *playingfield*. In the bottom row, after the annotator changes the label of the ground from *sand* to *snow*, our assistant corrects the label of the *rocks* in the background and also adds a *snowboard* as well as other snow regions.

4.3. Study with human annotators

We now verify whether the efficiency gains observed in simulation also transfer to human annotators.

Protocol. We randomly select 100 COCO validation images and have four humans annotate them. We compare polygon drawing, fluid annotation [5], and our system with all assistants. Importantly, we want to avoid measuring confounding effects, such as annotators being inherently faster than others, or being faster because they already saw the image before. We therefore make sure that each annotator annotates an equal number of images with each interface, while never annotating an image more than once. Additionally, we want to avoid measuring human label disagreement, which is a serious confounding factor: the COCO group had 5000 images annotated independently twice, and measured a human agreement of 0.54 panoptic score [2]. To rule out this factor, we show annotators the original COCO ground truth during annotation and ask them to reproduce it.

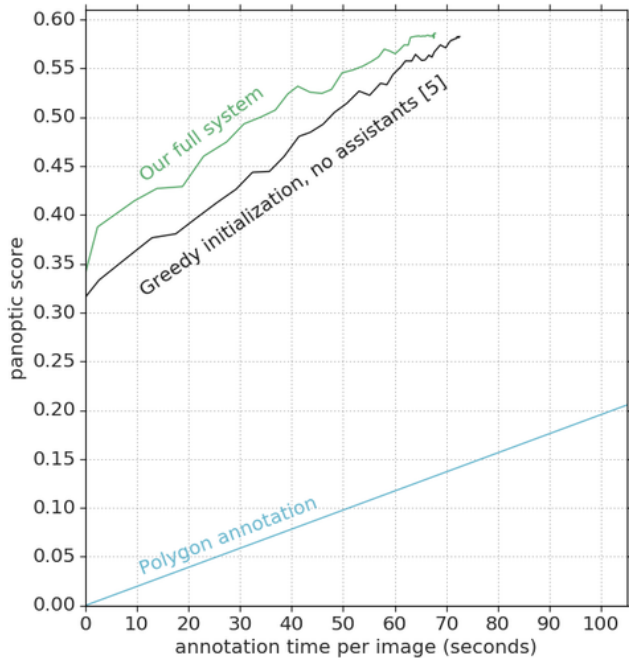


Figure 8. Results of user study on 100 images.

Thanks to all the precautions above, our study can measure time differences due to the interface only.

Results. Fig. 8 shows quality (panoptic score) as a function of human annotation time (in seconds). Overall, our method emerges as more efficient than [5] and polygon annotation. For example, after 40 seconds per image, the panoptic quality is 0.08 when doing polygon annotation, 0.48 for Fluid Annotation [5], and 0.53 for our full system. Thus, in this low-time-budget regime, our approach makes a further improvement over [5], which was already delivering much better annotations than polygon drawing. These reported improvements match what we observed in the simulation experiments (Sec. 4.2).

Polygon drawing requires 338s seconds on average to reach the end of the annotation process, compared to 67s for our method. Thus our method is $5\times$ faster. In terms of quality, it is important to note that even when the annotator draws polygons while looking at the original ground truth, they are unable to perfectly replicate the original annotation. In practice, they reach 0.74 panoptic quality, which can be seen as an upper-bound for this task. In comparison, when using our method, annotators reach 0.59 panoptic quality. Hence, our major speedup comes at the price of only a relatively small drop in annotation quality.

4.4. Annotating a new dataset

So far we applied our system to annotate new images from the same dataset it was trained on. In practice though, often one wants to annotate an entirely new dataset, with different appearance distribution and even new object and stuff classes. Here we explore this scenario by annotating

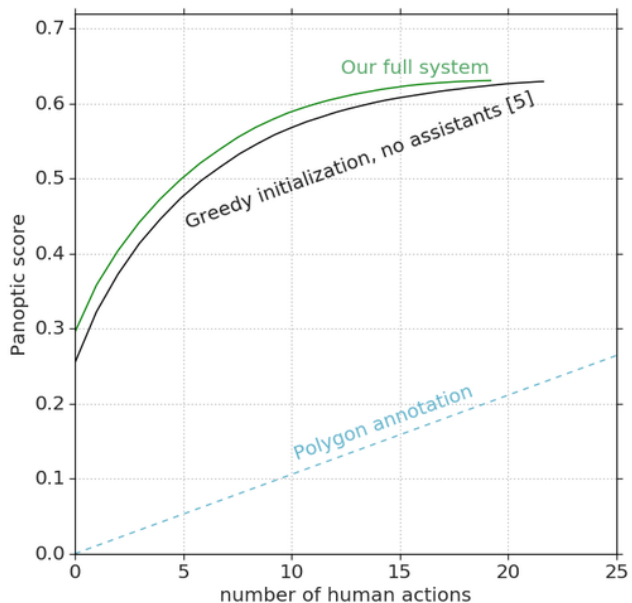


Figure 9. Simulated annotation results on ADE20k validation set.

ADE20k [59] (in simulation).

We fine-tune our system on a very small amount (5%, 1k images) of the ADE20k training set, so that it still brings a strong gain in overall annotation time. We use this data to train the underlying Mask-RCNN model for generating proposal sets and our assistants. We fine-tune models starting from those pre-trained on COCO, and use a 4-fold leave-one-out strategy where the assistants are trained on different images than those used to train Mask R-CNN. This trains better assistants while making efficient use of the limited training data.

We evaluate our system on the validation set of ADE20k (2k images). As Fig. 9 shows, our results in Sec. 4.2 generalize to annotating ADE20k: at 0.6 panoptic score, our system is 19% faster than [5]. Furthermore, our system reaches the final 0.63 panoptic quality 12% faster than [5].

5. Conclusions

We introduced a framework in which a human annotator and an automated assistant collaboratively annotate an image. The assistant intelligently reacts to human input based on context to annotate other parts of the image by itself. On the COCO panoptic dataset [14, 32, 38]: (1) in simulation we demonstrated that our system is 17%-27% faster than the recent interface [5]; (2) a human experiment confirms these improvements. At the same time, they show that our system is $5\times$ faster than polygon drawing, at the price of a small drop in accuracy. On ADE20k [59] we demonstrated that, starting from a very small amount of annotated data, our approach can be used to quickly annotate new datasets.

References

- [1] COCO panoptic dataset. <http://cocodataset.org/index.htm#panoptic-2018>. 5
- [2] COCO + Mapillary joint recognition challenge workshop. Workshop at ECCV, 2018. 7
- [3] D. Acuna, H. Ling, A. Kar, and S. Fidler. Efficient interactive annotation of segmentation datasets with polygon-rnn++. In *CVPR*, 2018. 2
- [4] E. Agustsson, J. Uijlings, and V. Ferrari. Interactive full image segmentation by considering all regions jointly. In *CVPR*, 2019. 2
- [5] M. Andriluka, J. R. R. Uijlings, and V. Ferrari. Fluid annotation: A human-machine collaboration interface for full image annotation. In *ACM Multimedia*, 2018. 1, 2, 3, 5, 6, 7, 8
- [6] X. Bai and G. Sapiro. Geodesic matting: A framework for fast interactive image and video segmentation and matting. *IJCV*, 2009. 1
- [7] D. Banica and C. Sminchisescu. Second-order constrained parametric proposals and sequential search-based structured prediction for semantic segmentation in rgb-d images. In *CVPR*, 2015. 5
- [8] D. Batra, A. Kowdle, D. Parikh, J. Luo, and T. Chen. Interactively co-segmenting topically related images with intelligent scribble guidance. *IJCV*, 2011. 1
- [9] R. Benenson, S. Popov, and V. Ferrari. Large-scale interactive object segmentation with human annotators. In *CVPR*, 2019. 1
- [10] A. Biswas and D. Parikh. Simultaneous active learning of classifiers & attributes via relative feedback. In *CVPR*, 2013. 2
- [11] Y. Boykov and M. P. Jolly. Interactive graph cuts for optimal boundary and region segmentation of objects in N-D images. In *ICCV*, 2001. 1
- [12] S. Branson, K. Hjörleifsson, and P. Perona. Active annotation translation. In *CVPR*, 2014. 2
- [13] S. Branson, C. Wah, F. Schroff, B. Babenko, P. Welinder, P. Perona, and S. Belongie. Visual recognition with humans in the loop. In *ECCV*, 2010. 2
- [14] H. Caesar, J. Uijlings, and V. Ferrari. COCO-Stuff: Thing and stuff classes in context. In *CVPR*, 2018. 1, 5, 6, 8
- [15] L. Castrejon, K. Kundu, R. Urtasun, and S. Fidler. Annotating object instances with a Polygon-RNN. In *CVPR*, 2017. 2
- [16] L.-C. Chen, G. Papandreou, I. Kokkinos, K. Murphy, and A. Yuille. Deeplab: Semantic image segmentation with deep convolutional nets, atrous convolution, and fully connected crfs. *IEEE Trans. on PAMI*, 2018. 1, 5
- [17] Y. Chen, J. Pont-Tuset, A. Montes, and L. Van Gool. Blazingly fast video object segmentation with pixel-wise metric learning. In *CVPR*, 2018. 1
- [18] M.-M. Cheng, V. A. Prisacariu, S. Zheng, P. H. S. Torr, and C. Rother. Denscut: Densely connected crfs for realtime grabcut. *Computer Graphics Forum*, 2015. 1
- [19] L. Cohen and R. Kimmel. Global minimum for active contour models: A minimal path approach. In *CVPR*, 1996. 2
- [20] M. Cordts, M. Omran, S. Ramos, T. Rehfeld, M. Enzweiler, R. Benenson, U. Franke, S. Roth, and B. Schiele. The cityscapes dataset for semantic urban scene understanding. In *CVPR*, 2016. 1
- [21] A. Criminisi, T. Sharp, C. Rother, and P. Perez. Geodesic image and video editing. In *ACM Trans. Gr.*, 2010. 1
- [22] H. Daumé III, J. Langford, and D. Marcu. Search-based structured prediction. *Machine Learning*, 75(3):297–325, 2009. 5
- [23] G. Gkioxari, A. Toshev, and N. Jaitly. Chained predictions using convolutional neural networks. In *ECCV*, 2016. 5
- [24] V. Gulshan, C. Rother, A. Criminisi, A. Blake, and A. Zisserman. Geodesic star convexity for interactive image segmentation. In *CVPR*, 2010. 1
- [25] K. He, G. Gkioxari, P. Dollár, and R. Girshick. Mask R-CNN. In *ICCV*, 2017. 3
- [26] K. He, X. Zhang, S. Ren, and J. Sun. Deep residual learning for image recognition. In *CVPR*, 2016. 4
- [27] G. Heitz and D. Koller. Learning spatial context: Using stuff to find things. In *ECCV*, 2008. 1, 5, 6
- [28] R. Hu, P. Dollár, K. He, T. Darrell, and R. Girshick. Learning to segment every thing. In *CVPR*, 2018. 4, 5
- [29] Y. Hu, A. Soltoggio, R. Lock, and S. Carter. A fully convolutional two-stream fusion network for interactive image segmentation. *Neural Networks*, 2019. 1, 5, 6
- [30] D. P. Kingma and J. L. Ba. Adam: A method for stochastic optimization. In *ICLR*, 2015. 5
- [31] T. N. Kipf and M. Welling. Semi-supervised classification with graph convolutional networks. In *ICLR*, 2017. 4
- [32] A. Kirillov, K. He, R. Girshick, C. Rother, and P. Dollar. Panoptic segmentation. In *CVPR*. 1, 3, 5, 6, 8
- [33] K. Konyushkova, J. Uijlings, C. Lampert, and V. Ferrari. Learning intelligent dialogs for bounding box annotation. In *CVPR*, 2018. 2
- [34] H. Le, L. Mai, B. Price, S. Cohen, H. Jin, and F. Liu. Interactive boundary prediction for object selection. In *ECCV*, 2018. 1, 2
- [35] Z. Li, Q. Chen, and V. Koltun. Interactive image segmentation with latent diversity. In *CVPR*, 2018. 1
- [36] J. Liew, Y. Wei, W. Xiong, S.-H. Ong, and J. Feng. Regional interactive image segmentation networks. In *ICCV*, 2017. 1
- [37] D. Lin, Y. Ji, D. Lischinski, D. Cohen, and H. Huang. Multi-scale context intertwining for semantic segmentation. In *ECCV*, 2019. 1, 5, 6
- [38] T.-Y. Lin, M. Maire, S. Belongie, J. Hays, P. Perona, D. Ramanan, P. Dollár, and C. Zitnick. Microsoft COCO: Common objects in context. In *ECCV*, 2014. 1, 5, 6, 8
- [39] J. Long, E. Shelhamer, and T. Darrell. Fully convolutional networks for semantic segmentation. In *CVPR*, 2015. 1, 5
- [40] S. Mahadevan, P. Voigtlaender, and B. Leibe. Iteratively trained interactive segmentation. In *BMVC*, 2018. 1
- [41] K.-K. Maninis, S. Caelles, J. Pont-Tuset, and L. Van Gool. Deep extreme cut: From extreme points to object segmentation. In *CVPR*, 2018. 1
- [42] D. Modolo, A. Vezhnevets, and V. Ferrari. Context forest for object class detection. In *BMVC*, 2015. 1, 6

- [43] R. Mottaghi, X. Chen, X. Liu, N.-G. Cho, S.-W. Lee, S. Fidler, R. Urtasun, and A. Yuille. The role of context for object detection and semantic segmentation in the wild. In *CVPR*, 2014. [5](#)
- [44] K. Murphy, A. Torralba, and W. T. Freeman. Using the forest to see the trees: A graphical model relating features, objects, and scenes. In *NIPS*, 2003. [1](#), [5](#), [6](#)
- [45] N. S. Nagaraja, F. R. Schmidt, and T. Brox. Video segmentation with just a few strokes. In *ICCV*, 2015. [1](#)
- [46] D. P. Papadopoulos, J. R. Uijlings, F. Keller, and V. Ferrari. Extreme clicking for efficient object annotation. In *ICCV*, 2017. [2](#)
- [47] D. P. Papadopoulos, J. R. Uijlings, F. Keller, and V. Ferrari. We don't need no bounding-boxes: Training object class detectors using only human verification. In *CVPR*, 2016. [2](#)
- [48] A. Parkash and D. Parikh. Attributes for classifier feedback. In *ECCV*, 2012. [2](#)
- [49] A. Rabinovich, A. Vedaldi, C. Galleguillos, E. Wiewiora, and S. Belongie. Objects in context. In *ICCV*, 2007. [1](#), [5](#), [6](#)
- [50] C. Rother, V. Kolmogorov, and A. Blake. Grabcut: Interactive foreground extraction using iterated graph cuts. In *SIGGRAPH*, 2004. [1](#)
- [51] C. Rupprecht, I. Laina, N. Navab, G. D. Hager, and F. Tombari. Guide me: Interacting with deep networks. In *CVPR*, 2018. [2](#)
- [52] O. Russakovsky, L.-J. Li, and L. Fei-Fei. Best of both worlds: human-machine collaboration for object annotation. In *CVPR*, 2015. [2](#)
- [53] A. Santoro, D. Raposo, D. G. Barrett, M. Malinowski, R. Pascanu, P. Battaglia, and T. Lillicrap. A simple neural network module for relational reasoning. In *NIPS*. 2017. [5](#)
- [54] H. Su, J. Deng, and L. Fei-Fei. Crowdsourcing annotations for visual object detection. In *AAAI Human Computation Workshop*, 2012. [2](#)
- [55] J. Tighe and S. Lazebnik. Understanding scenes on many levels. In *ICCV*, 2011. [1](#), [5](#), [6](#)
- [56] S. Vijayanarasimhan and K. Grauman. What's it going to cost you?: Predicting effort vs. informativeness for multi-label image annotations. In *CVPR*, 2009. [2](#)
- [57] C. Wah, G. Van Horn, S. Branson, S. Maji, P. Perona, and S. Belongie. Similarity comparisons for interactive fine-grained categorization. In *CVPR*, 2014. [2](#)
- [58] N. Xu, B. Price, S. Cohen, J. Yang, and T. Huang. Deep interactive object selection. In *CVPR*, 2016. [1](#)
- [59] B. Zhou, H. Zhao, X. Puig, T. Xiao, S. Fidler, A. Barriuso, and A. Torralba. Semantic understanding of scenes through the ade20k dataset. *IJCV*, 2019. [1](#), [8](#)